

DETERMINATION OF DYNAMIC STRESS INTENSITY FACTOR IN FGM PLATES BY MLPG METHOD^{*}

A. ABDOLLAHIFAR AND M. R. NAMI^{**}

Dept. of Mechanical Eng., Shiraz University, Shiraz, I. R. of Iran
Email: nami@shirazu.ac.ir

Abstract– In this paper, the meshless local Petrov-Galerkin (MLPG) method is used to analyze the dynamic fracture of an isotropic FGM plate containing a center crack. The dynamic stress intensity factors are studied under the influence of various non-homogeneity ratios. Both the moving least square (MLS) and the direct method have been applied to estimate the shape function and to impose the essential boundary conditions. The enriched weight function method is used to simulate the displacement and stress field around the crack tip. Normalized dynamic stress intensity factors (NDSIF) are calculated using the path independent integral, J^* , which is formulated for the non-homogeneous material.

To validate the method, the homogenous center cracked plate problem is analyzed. The obtained results show good agreement between the analytical solution and the MLPG results for homogenous material. After validation, a center cracked plate made of FGM with two different material gradations (along and normal to the crack length) and three different lengths of FGM zone under the effect of step load are considered, and the following six distinct problems are studied here.

Keywords– MLPG, FGM, dynamic stress intensity factor (DSIF), J^* integral, mix mode, crack

1. INTRODUCTION

Functionally graded materials (FGMs) are a new generation of engineered materials that contain a continuous, or discontinuous, gradient in composition and microstructure. Such gradients can be tailored to meet specific needs while providing the best use of composite components [1]. The concept of FGMs was proposed in 1984 by material scientists in the Sendai area, Japan, as a means of preparing thermal barrier materials [2]. This technology solves the problem of sharp interface between two dissimilar materials. The absence of sharp interfaces in continually graded FGMs greatly reduces material property mismatch, which has been found to improve resistance to interfacial delamination and fatigue crack propagation [3]. Crack problems in FGMs have received considerable attention from a number of researchers around the world. In [4] it was shown that the J integral introduced by Rice concerning non-homogeneous material is not path-independent. Subsequently, Eischen has introduced a new path independent integral J^* for elastostatic problems [5]. In this mentioned paper, the FEM method was used to solve the problem. In [6] the J^* integral concept is implemented to element free Galerkin (EFG) method for FGM problems.

Although the analytical study of non-homogeneous problems provides the closed-form solutions, these solutions are limited to the problems with simple geometries, certain types of gradation and the special loading cases. For this reason, the analytical method is not applicable to most of the problems and

^{*}Received by the editors October 9, 2012; Accepted December 7, 2013.

^{**}Corresponding author

numerical approaches such as finite element method, boundary element method, meshless method [7], etc. are inevitable. In [8] a simple method was presented to determine the numerical value of stress intensity factors. The effect of non-homogeneity on the numerical calculation of J integral was also investigated in this research and accurate results were obtained by employing very small elements around the crack. Numerical analysis of crack-tip fields in functionally graded materials with a crack normal to the elastic gradient was also performed by Marur et al. in [9].

In the past two decades, Meshless methods have attracted considerable attention in solving boundary value problems. The main feature of these methods is rooted in the fact that only a set of scattered nodes in the physical domain is required to approximate the solutions, and the nodes do not need to be connected to form closed polygons. In contrast to the finite element method, Meshless methods can save the preprocessing work of mesh generation, as no element is required for the whole model [10]. A “true meshless” method is presented in [11] that does not require any mesh for the integration of the weak formulations. This method is based on a local weak form in conjunction with the moving least squares (MLS) approximation and is known as the meshless local Petrov–Galerkin (MLPG) method. Integration for each node is implemented only over a local quadrature domain that is often a regularly shaped sub-domain. The MLPG method has been used for solving various engineering problems such as fracture mechanics [12], elasto-dynamic [13] and dynamic fracture [14] problems. In [15], the six different types of MLPG methods were introduced on the basis of different test functions. A new meshless local Petrov–Galerkin method has also been introduced in [16] to solve the elastostatic problems.

MLPG was also used for analyzing the 2-D crack in FGM with MLS technique and step test function [17]. Cracks in isotropic functionally graded materials under static load are analyzed by MLPG in [18]. Effect of angle between the material gradation direction and crack length on mixed-mode stress intensity factor of FGM plates under static load is investigated by MLPG method in [19]. Effect of FGM gradation direction on mixed-mode crack initiation angle under static and dynamic load is investigated by MLPG method in [20]. Sladek et al. [21, 22] used MLPG and the modified interaction integral for the evaluation of stress intensity factors in FGMs. Recently, the dynamic fracture of anisotropic FGMs has been studied using the MLPG method [23, 24]. For more information on dynamic fractures of FGMs, see also [25].

In this paper, MLPG method is used to analyze the dynamic fracture of an isotropic FGM plate that contains a center crack. The time history of normalized dynamic stress intensity factor (NDSIF) in the center cracked plate with two different material gradations (along and normal to the crack) and three different FGM zones (10%, half and full of plate length) under step load are explored.

Moving least square (MLS) has been applied to estimate the shape function. The direct method [26] is used to impose the essential boundary conditions. Enriched weight function method is used to simulate the displacement and stress field around the crack tip. The dynamic stress intensity factors are calculated using the path independent J^* integrals, which are formulated for the non-homogeneous material under dynamic condition.

2. THE MLPG METHOD

In this section, the MLS approximation and the weak formulation, on which the MLPG method is based, are introduced. The following derivation of the MLPG formulation is given by [10, 11].

a) *MLS scheme*

The MLS approximation is widely used in meshless methods for constructing meshless shape functions. The interpolation function $u^h(x)$ of a field variable $u(x)$ is defined in a domain Ω_x by

$$u^h(x) = \sum_{I=1}^N \phi_I(x) u_I \quad (1)$$

where, N is the number of nodes in the support domain of point x , for which the weight function is nonzero, u_I is the nodal parameters of the field function for node I , in the support domain, and $\phi_I(x)$ is the shape function for the node number I , defined by

$$\phi_I(x) = \sum_j^m p_j(x) (\mathbf{A}^{-1}(x) \mathbf{B}(x))_{jI} = \mathbf{P}^T \mathbf{A}^{-1} \mathbf{B}_I \quad (2)$$

where, \mathbf{P}^T is a vector of complete monomial basis of order m . For the 2-D problems, \mathbf{P}^T is given by

$$\mathbf{P}^T(\mathbf{x}) = \{1, x, y, x^2, y^2, \dots, x^m, y^m\} \quad (3)$$

and $\mathbf{A}(x)$ is called the weighted moment matrix, defined by

$$\mathbf{A}(x) = \sum_I^N W_I(x) \mathbf{P}(x_I) \mathbf{P}^T(x_I) \quad (4)$$

where, $W_I(x)$ is the weight function of node I . In this paper, the Gaussian weight function

$$w(x) = \frac{e^{-\frac{d^2}{c}} - e^{-\frac{r^2}{c}}}{1 - e^{-\frac{r^2}{c}}} (1 - H[d - r]) \quad (5)$$

where, $d = \|x - x^a\|$ is the distance between the sampling point x and node x^a , c is a constant controlling the shape of the weight function, r is the radius of the circular support domain of the weight function and H is the Heaviside unit step function.

b) Weak formulation and discretization

For a two-dimensional elastodynamic problem on the domain Ω bounded by the boundary Γ , the governing equation, boundary conditions and initial conditions are respectively given by

$$\nabla \cdot \boldsymbol{\sigma} + \mathbf{b} = \rho \ddot{\mathbf{u}} + \eta \dot{\mathbf{u}} \quad (6)$$

$$\mathbf{u} = \bar{\mathbf{u}} \quad \text{on} \quad \Gamma_u \quad \text{Essential boundary condition}$$

$$\boldsymbol{\sigma} \cdot \mathbf{n} = \bar{\mathbf{t}} \quad \text{on} \quad \Gamma_t \quad \text{Natural boundary condition} \quad (7)$$

$$\mathbf{u}(\mathbf{x}, t_0) = \mathbf{u}_0(\mathbf{x}) \quad \mathbf{x} \in \Omega \quad \text{Displacement initial condition}$$

$$\dot{\mathbf{u}}(\mathbf{x}, t_0) = \mathbf{v}_0(\mathbf{x}) \quad \mathbf{x} \in \Omega \quad \text{Velocity initial condition}$$

where, $\boldsymbol{\sigma}$ is the stress tensor, \mathbf{b} is the body force vector, ρ is the mass density, η is the damping coefficient, \mathbf{u} is the displacement vector, $\ddot{\mathbf{u}} = \partial^2 \mathbf{u} / \partial t^2$ is the acceleration vector, $\dot{\mathbf{u}} = \partial \mathbf{u} / \partial t$ is the velocity vector, \mathbf{n} is the unit outward normal to the boundary Γ , and $\bar{\mathbf{u}}$, $\bar{\mathbf{t}}$, \mathbf{u}_0 and \mathbf{v}_0 are the prescribed displacements, tractions, and the initial displacements and velocities, respectively.

A generalized local weak form of (7) over a local sub-domain Ω_Q can be written as

$$\int_{\Omega_Q} (\nabla \cdot \boldsymbol{\sigma} + \mathbf{b} - \rho \ddot{\mathbf{u}} - \eta \dot{\mathbf{u}}) W_I d\Omega = 0 \quad (8)$$

where, W_I is the test function defined in (5).

Using the divergence theorem and substituting the MLS approximation (1) into (8) and rearranging the result, leads to

$$\int_{\Omega_Q} (\mathbf{W}_I \rho \ddot{\mathbf{u}} + \mathbf{W}_I \eta \dot{\mathbf{u}} + \mathbf{V}_I^T \boldsymbol{\sigma}) d\Omega - \int_{\Gamma_u} \mathbf{W}_I \mathbf{t} d\Gamma = \int_{\Gamma_t} \mathbf{W}_I \bar{\mathbf{t}} d\Gamma + \int_{\Omega_Q} \mathbf{W}_I \mathbf{b} d\Omega \quad (9)$$

where

$$\boldsymbol{\sigma}^T = \begin{bmatrix} \sigma_{xx} & \sigma_{yy} & \sigma_{xy} \end{bmatrix} \quad (10)$$

$$\mathbf{b}^T = \begin{bmatrix} b_x & b_y \end{bmatrix} \quad (11)$$

$$\mathbf{V}_I = \begin{bmatrix} W_{I,x} & 0 \\ 0 & W_{I,y} \\ W_{I,y} & W_{I,x} \end{bmatrix} \quad (12)$$

$$\mathbf{W}_I = \begin{bmatrix} W_I & 0 \\ 0 & W_I \end{bmatrix} \quad (13)$$

Using the Hooke's law for a linear elastic solid, one obtains

$$\boldsymbol{\sigma} = \mathbf{c} \boldsymbol{\varepsilon} = \mathbf{c} \begin{bmatrix} \frac{\partial}{\partial x} & 0 \\ 0 & \frac{\partial}{\partial y} \\ \frac{\partial}{\partial y} & \frac{\partial}{\partial x} \end{bmatrix} \left\{ \sum_j^N \boldsymbol{\Phi}_j \mathbf{u}_j \right\} = \mathbf{c} \sum_j^N \mathbf{B}_j \mathbf{u}_j \quad (14)$$

where

$$\boldsymbol{\Phi}_j = \begin{bmatrix} \phi_j & 0 \\ 0 & \phi_j \end{bmatrix} \quad (15)$$

and the compliance matrix \mathbf{c} for a homogeneous isotropic solid is defined as

$$\mathbf{c} = \frac{E^*}{1-\nu^{*2}} \begin{bmatrix} 1 & \nu^* & 0 \\ \nu^* & 1 & 0 \\ 0 & 0 & (1-\nu^*)/2 \end{bmatrix} \quad (16)$$

where, $\nu^* = \nu$, $E^* = E$ for the plane stress condition and $\nu^* = \nu / (1-\nu^2)$, $E^* = E / (1-\nu^2)$ for the plane strain condition. The tractions \mathbf{t} at a point \mathbf{x} can be written as

$$\mathbf{t} = \begin{bmatrix} n_x & 0 & n_y \\ 0 & n_y & n_x \end{bmatrix} \boldsymbol{\sigma} = \mathbf{n} \mathbf{c} \sum_j^N \mathbf{B}_j \mathbf{u}_j \quad (17)$$

where, \mathbf{n} is the unit outward normal vector on the boundary Γ as

$$\mathbf{n} = \begin{bmatrix} n_x & 0 & n_y \\ 0 & n_y & n_x \end{bmatrix} \quad (18)$$

Substitution of (14) - (18) into (9) leads to the following discrete systems of linear equations for the I th node:

$$\int_{\Omega_Q} (\rho \mathbf{W}_I \sum_J^N \Phi_J \ddot{\mathbf{u}}_J + \eta \mathbf{W}_I \sum_J^N \Phi_J \dot{\mathbf{u}}_J + \mathbf{V}_I^T \mathbf{c} \sum_J^N \mathbf{B}_J \mathbf{u}_J) d\Omega - \int_{\Gamma_u} \mathbf{W}_I \mathbf{n} \mathbf{c} \sum_J^N \mathbf{B}_J \mathbf{u}_J d\Gamma = \int_{\Gamma_t} \mathbf{W}_I \bar{\mathbf{t}} d\Gamma + \int_{\Omega_Q} \mathbf{W}_I \mathbf{b} d\Omega \quad (19)$$

The matrix form of the above equation can be written as

$$\sum_{j=1}^N (\mathbf{M}_{Ij} \ddot{\mathbf{u}}_j + \mathbf{C}_{Ij} \dot{\mathbf{u}}_j + \mathbf{K}_{Ij} \mathbf{u}_j) = \mathbf{f}_I \quad (20)$$

where the nodal stiffness, damping and mass matrices and the nodal force vector are defined, respectively, as

$$\mathbf{K}_{Ij} = \int_{\Omega_Q} \mathbf{V}_I^T \mathbf{c} \mathbf{B}_J d\Omega - \int_{\Gamma_u} \mathbf{W}_I \mathbf{n} \mathbf{c} \mathbf{B}_J d\Gamma \quad (21)$$

$$\mathbf{C}_{Ij} = \int_{\Omega_Q} \eta \mathbf{W}_I \Phi_J d\Omega \quad (22)$$

$$\mathbf{M}_{Ij} = \int_{\Omega_Q} \rho \mathbf{W}_I \Phi_J d\Omega \quad (23)$$

$$\mathbf{f}_I = \int_{\Gamma_{Qt}} \mathbf{W}_I \bar{\mathbf{t}} d\Gamma + \int_{\Omega_Q} \mathbf{W}_I \mathbf{b} d\Omega \quad (24)$$

To evaluate the integrals in equations (21-24) Gauss–Legendre quadrature rule could be used. This is a simple and easy to use method but is relatively time consuming. The *analytical integrations*, which reduces the computational time is also presented in [27, 28 and 29]. In the present paper, because of the nature of the studied cases, the Gauss–Legendre method was preferred, and so was applied to the model.

c) The direct method [26, 10]

Denote the prescribed displacements on the essential boundary at node I as

$$\begin{cases} u_I = \bar{u}_I \\ v_I = \bar{v}_I \end{cases} \quad (25)$$

According to (1), the essential boundary condition for node I will be directly imposed by replacing (2I-1)th and 2Ith rows of the stiffness matrix and the force vector with

$$\begin{bmatrix} \phi_1 & 0 & \phi_2 & 0 & \dots & \phi_N & 0 \\ 0 & \phi_1 & 0 & \phi_2 & \dots & 0 & \phi_N \end{bmatrix} \text{ and } \begin{bmatrix} \bar{u}_I \\ \bar{v}_I \end{bmatrix} \text{ respectively.}$$

3. THE TIME INTEGRATION SCHEME

a) Central difference method [10]

The central difference method (CDM) consists of expressing the velocity and acceleration at time t in terms of the displacement at time $t - \Delta t$, t and $t + \Delta t$ using central finite difference formulation:

$$\ddot{\mathbf{u}}_t = \frac{1}{\Delta t^2} (\mathbf{u}_{t-\Delta t} - 2\mathbf{u}_t + \mathbf{u}_{t+\Delta t}) \quad (26)$$

$$\dot{\mathbf{u}}_t = \frac{1}{2\Delta t} (-\mathbf{u}_{t-\Delta t} + \mathbf{u}_{t+\Delta t}) \quad (27)$$

where Δt is the time step. Then, the response at time $t + \Delta t$ is obtained by evaluating the equation of motion at time t . The CDM method is conditionally stable so that the solution is stable when the time step is sufficiently small.

b) The Newmark method [10]

The Newmark family of methods can be used to integrate (20). The recursive relations for displacements and velocities at times $t - \Delta t$ and t are given by

$$\mathbf{u}_t = \mathbf{u}_{t-\Delta t} + \Delta t \dot{\mathbf{u}}_{t-\Delta t} + \frac{\Delta t^2}{2} \ddot{\mathbf{u}}_{t-\Delta t} + \beta \Delta t^3 \ddot{\mathbf{u}}_t \quad (28)$$

$$\dot{\mathbf{u}}_t = \dot{\mathbf{u}}_{t-\Delta t} + \Delta t \ddot{\mathbf{u}}_{t-\Delta t} + \gamma \Delta t^2 \ddot{\mathbf{u}}_t \quad (29)$$

By letting

$$\ddot{\mathbf{u}}_t = \frac{\ddot{\mathbf{u}}_t - \ddot{\mathbf{u}}_{t-\Delta t}}{\Delta t} \quad (30)$$

in (28) and (29), one gets

$$\mathbf{u}_t = \mathbf{u}_{t-\Delta t} + \Delta t \dot{\mathbf{u}}_{t-\Delta t} + \left(\frac{1}{2} - \beta \right) \Delta t^2 \ddot{\mathbf{u}}_{t-\Delta t} + \beta \Delta t^2 \ddot{\mathbf{u}}_t \quad (31)$$

$$\dot{\mathbf{u}}_t = \dot{\mathbf{u}}_{t-\Delta t} + (1 - \gamma) \Delta t \ddot{\mathbf{u}}_{t-\Delta t} + \gamma \Delta t \ddot{\mathbf{u}}_t \quad (32)$$

where γ and β are the parameters which control the stability and the accuracy of the time integration scheme. In this paper, $\beta = 0.25$ and $\gamma = 0.5$ are used for all calculations.

Writing (20) at time $t_{k+1} = (k+1)\Delta t$ and substituting from (31) and (32) yields the following system of equations:

$$\begin{aligned} (b_1 \mathbf{M} + b_4 \mathbf{C} + \mathbf{K}) \mathbf{u}_t &= \mathbf{F}_t + \\ \mathbf{M} (b_1 \mathbf{u}_{t-\Delta t} - b_2 \dot{\mathbf{u}}_{t-\Delta t} - b_3 \ddot{\mathbf{u}}_{t-\Delta t}) &+ \\ \mathbf{C} (b_4 \mathbf{u}_{t-\Delta t} - b_5 \dot{\mathbf{u}}_{t-\Delta t} - b_6 \ddot{\mathbf{u}}_{t-\Delta t}) & \end{aligned} \quad (33)$$

where

$$\begin{aligned} b_1 &= \frac{1}{\beta \Delta t^2} & b_2 &= -\frac{1}{\beta \Delta t} & b_3 &= 1 - \frac{1}{2\beta} \\ b_4 &= \gamma \Delta t b_1 & b_5 &= 1 + \gamma \Delta t b_2 & b_6 &= (1 - \gamma + \gamma b_3) \Delta t \end{aligned} \quad (34)$$

In this paper, the Newmark method is used to solve discrete dynamic equations.

4. SOLVING FRACTURE MECHANICS PROBLEMS USING THE MLPG METHOD

To solve the fracture mechanics problems using the meshless methods, it is necessary to increase the numbers of nodes in neighborhood of the crack tip, causing an increase in computation time. One of the most commonly used methods to avoid this problem is enriching base functions. In this method, the following functions are added into the monomial base functions [30].

$$\left\{ \sqrt{r} \cos \frac{\theta}{2}, \sqrt{r} \sin \frac{\theta}{2}, \sqrt{r} \cos \frac{\theta}{2} \sin \theta, \sqrt{r} \sin \frac{\theta}{2} \cos \theta \right\} \quad (35)$$

where, (r, θ) is the cylindrical coordinate with origin located at the crack tip and the positive angle measured counter-clockwise from the axis of the crack.

Despite the simplicity in the method of enriching the base functions, using it causes an increase in the number of base functions and consequently an increase in the time required for calculating the shape function.

The displacement field around the crack tip is normally discontinuous, but in meshless methods, continuous test functions and their derivatives are always used to simulate the problem. Therefore, various methods have been developed to create discontinuity of displacement field around the crack tip, like visibility [31] and diffraction criteria [32].

In this paper, the analysis of fracture mechanics problems has been carried out substituting functions (36) with test Function (5).

$$\begin{aligned} \nu_1(\mathbf{x}) &= \sqrt{r} \cos(\theta/2) * W_r(d) \\ \nu_2(\mathbf{x}) &= \sqrt{r} [1 + \sin(\theta/2)] * W_r(d) \\ \nu_3(\mathbf{x}) &= \sqrt{r} [1 - \sin(\theta/2)] * W_r(d) \end{aligned} \quad (36)$$

These weight functions have the same behavior of \sqrt{r} near the crack tip. The functions $\nu_2(\mathbf{x})$ and $\nu_3(\mathbf{x})$ are two -valued functions and cause the discontinuity of shape function and displacement field along the crack [33]. Regarding the mentioned qualities, the weight function $\nu_1(\mathbf{x})$ in the front points of the crack, the weight function $\nu_2(\mathbf{x})$ in the upper points of the crack, and weight function $\nu_3(\mathbf{x})$ in the lower points of the crack are usable. Due to the limitlessness of the above functions derivatives in the definite location of the crack tip, three nodes in the front, bottom and top of the crack and near the crack tip have been used. Therefore, using the enriched weight functions, it is not necessary to develop the base functions and use the rectification methods of displacement field.

5. FRACTURE IN FUNCTIONALLY GRADED MATERIALS

The elastic properties at any point in FGMs can be assumed to be the same in all directions, hence at the continuum level FGMs can be considered as isotropic nonhomogeneous solids [3]. The elastic modulus and density variations can be assumed as [3]:

$$\begin{aligned} E(x) &= E_1 \exp(\beta x), \quad \beta = \ln(E_1 / E_2) / L, \\ E_1 &= E(0), \quad E_2 = E(L) \end{aligned} \quad (37)$$

$$\begin{aligned} \rho(x) &= \rho_1 \exp(\beta x), \\ \rho_1 &= \rho(0), \quad \rho_2 = \rho(L) \end{aligned}$$

where β is a non-homogeneity factor.

The J integral method is commonly used to evaluate the SIFs in homogenous materials [4], but is path dependent for non-homogeneous cases. To overcome the challenge, Eischen has introduced a new path independent integral J^* for elastostatic problems [5]. For elastostatic and elastodynamic problems, Sladek et al. [21, 22] modified interaction integral for the evaluation of stress intensity factors in FGMs. In

this paper the J^* integral formulation for elastodynamic problems is presented using the same procedure as [5, 21].

The elastic strain energy density function W for nonhomogeneous solid is defined by

$$W = W(\varepsilon_{ij}, x_i) \quad (38)$$

Note that when the material is homogeneous, the strain energy function will be $W = W(\varepsilon_{ij})$. For nonhomogeneous elastic solid elastic, strain energy can be written in the following form:

$$W = \frac{1}{2} \sigma_{ij} \varepsilon_{ij} = \frac{1}{2} c_{ijkl} \varepsilon_{ij} \varepsilon_{kl} \quad (39)$$

The gradient of strain energy density is given as

$$\frac{\partial W}{\partial x_k} = \frac{\partial W}{\partial \varepsilon_{ij}} \frac{\partial \varepsilon_{ij}}{\partial x_k} + \left(\frac{\partial W}{\partial x_k} \right) \Big|_{\text{explicit}} \quad (40)$$

where the term for the ‘‘explicit’’ derivative of the strain energy density for non-homogeneous materials becomes

$$\left(\frac{\partial W}{\partial x_k} \right) \Big|_{\text{explicit}} = \frac{1}{2} c_{ijlm,k} \varepsilon_{ij} \varepsilon_{lm} \quad (41)$$

Using the symmetry properties of the strain tensor, one obtains

$$\frac{\partial W}{\partial \varepsilon_{ij}} = \frac{1}{2} (c_{ijkl} \varepsilon_{ij} + c_{ijkl} \varepsilon_{kl}) \Rightarrow \frac{\partial W}{\partial \varepsilon_{ij}} = c_{ijkl} \varepsilon_{ij} = \sigma_{ij} \quad (42)$$

Using the strain-displacement relations, one obtains

$$\frac{\partial \varepsilon_{ij}}{\partial x_k} = \frac{\partial}{\partial x_k} \left(\frac{1}{2} \left(\frac{\partial u_i}{\partial x_j} + \frac{\partial u_j}{\partial x_i} \right) \right) = \frac{1}{2} \left(\frac{\partial^2 u_i}{\partial x_j \partial x_k} + \frac{\partial^2 u_j}{\partial x_i \partial x_k} \right) \quad (43)$$

Hence, by using the symmetry properties of the stress tensor

$$\frac{\partial W}{\partial \varepsilon_{ij}} \frac{\partial \varepsilon_{ij}}{\partial x_k} = \frac{1}{2} \sigma_{ij} \left(\frac{\partial^2 u_i}{\partial x_j \partial x_k} + \frac{\partial^2 u_j}{\partial x_i \partial x_k} \right) = \sigma_{ij} \frac{\partial^2 u_i}{\partial x_j \partial x_k} \quad (44)$$

The above equation can be written as follows

$$\frac{\partial W}{\partial \varepsilon_{ij}} \frac{\partial \varepsilon_{ij}}{\partial x_k} = \sigma_{ij} \frac{\partial^2 u_i}{\partial x_j \partial x_k} = \frac{\partial}{\partial x_j} \left(\sigma_{ij} \frac{\partial u_i}{\partial x_k} \right) - \frac{\partial \sigma_{ij}}{\partial x_j} \frac{\partial u_i}{\partial x_k} \quad (45)$$

Substituting (45) to (40) yields

$$\frac{\partial}{\partial x_j} \left(W \delta_{kj} + \sigma_{ij} \frac{\partial u_i}{\partial x_k} \right) = - \frac{\partial \sigma_{ij}}{\partial x_j} \frac{\partial u_i}{\partial x_k} + \left(\frac{\partial W}{\partial x_k} \right) \Big|_{\text{explicit}} \quad (46)$$

Substituting the equilibrium equations $\left(\frac{\partial \sigma_{ij}}{\partial x_j} = \rho \ddot{u}_i + \eta \dot{u}_i - b_i \right)$ into the above equations, leads to

$$\frac{\partial}{\partial x_j} (W \delta_{kj} + \sigma_{ij} \frac{\partial u_i}{\partial x_k}) = (b_i - \rho \ddot{u}_i - \eta \dot{u}_i) \frac{\partial u_i}{\partial x_k} + \left(\frac{\partial W}{\partial x_k} \right) \Big|_{\text{explicit}} \quad (47)$$

where δ_{kj} is the Kronecker delta function.

An integral form of (47) proves necessary for application in computational work. A regular bounded region Ω enclosed by a curve Γ whose unit outward normal vector is \mathbf{n} is considered. Applying the divergence theorem results in the following equation:

$$\int_{\Gamma} (W \delta_{kj} + \sigma_{ij} \frac{\partial u_i}{\partial x_k}) n_j d\Gamma = \int_{\Omega} (b_i - \rho \ddot{u}_i - \eta \dot{u}_i) \frac{\partial u_i}{\partial x_k} d\Omega + \int_{\Omega} \left(\frac{\partial W}{\partial x_k} \right) \Big|_{\text{explicit}} d\Omega \quad (48)$$

In applying the divergence theorem it was assumed that field quantities were continuous, bounded, and generally differentiable on Ω . Since the stress and strain fields are singular at the crack tip and the displacements are discontinuous across both crack-surfaces, a cut-off along the crack with a small region in the vicinity of the crack-tip Ω_ϵ has to be excluded. The radius of Ω_ϵ is considered to be very small and shrunk to zero in the limiting process. Tractions are permitted to act on the crack surfaces. The crack is parallel to the x_1 axis of the local Cartesian coordinate system. So, the above equation can be written as (see Fig1):

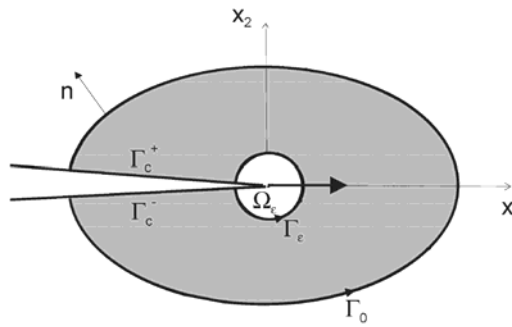


Fig. 1. J* Integration paths

$$\int_{\Gamma_\epsilon} (W \delta_{kj} + \sigma_{ij} \frac{\partial u_i}{\partial x_k}) n_j d\Gamma = \int_{\Gamma_0} (W \delta_{kj} + \sigma_{ij} \frac{\partial u_i}{\partial x_k}) n_j d\Gamma + \int_{\Gamma_c^+} (W^+ - W^-) \delta_{k2} d\Gamma - \lim_{\epsilon \rightarrow 0} \left\{ \int_{\Omega_0 - \Omega_\epsilon} (b_i - \rho \ddot{u}_i - \eta \dot{u}_i) \frac{\partial u_i}{\partial x_k} d\Omega - \int_{\Omega_0 - \Omega_\epsilon} \left(\frac{\partial W}{\partial x_k} \right) \Big|_{\text{explicit}} d\Omega \right\} \quad (49)$$

The left side of the above equation is identical to the definition of the J*.

Let k=1, then

$$J_1^* = \int_{\Gamma_0} W n_1 + \sigma_{ij} \frac{\partial u_i}{\partial x_1} n_j d\Gamma - \lim_{\epsilon \rightarrow 0} \left\{ \int_{\Omega_0 - \Omega_\epsilon} (b_i - \rho \ddot{u}_i - \eta \dot{u}_i) \frac{\partial u_i}{\partial x_1} d\Omega - \int_{\Omega_0 - \Omega_\epsilon} \left(\frac{\partial W}{\partial x_1} \right) \Big|_{\text{explicit}} d\Omega \right\} \quad (50)$$

Let k=2, then

$$J_2^* = \int_{\Gamma_0} W n_2 + \sigma_{ij} \frac{\partial u_i}{\partial x_2} n_j d\Gamma + \int_{\Gamma_c^+} (W^+ - W^-) d\Gamma - \lim_{\epsilon \rightarrow 0} \left\{ \int_{\Omega_0 - \Omega_\epsilon} (b_i - \rho \ddot{u}_i - \eta \dot{u}_i) \frac{\partial u_i}{\partial x_2} d\Omega - \int_{\Omega_0 - \Omega_\epsilon} \left(\frac{\partial W}{\partial x_2} \right) \Big|_{\text{explicit}} d\Omega \right\} \quad (51)$$

According to Eischen's work, K_I and K_{II} could be defined as follows:

$$K_I = \left\{ \frac{E_{tip}^* J_1^*}{2} \left[1 \pm \left(1 - \left(\frac{J_2^*}{J_1^*} \right)^2 \right)^{\frac{1}{2}} \right] \right\}^{\frac{1}{2}} \tag{52}$$

$$K_{II} = \pm \left\{ \frac{E_{tip}^* J_1^*}{2} \left[1 \mp \left(1 - \left(\frac{J_2^*}{J_1^*} \right)^2 \right)^{\frac{1}{2}} \right] \right\}^{\frac{1}{2}} \tag{53}$$

where E_{tip}^* is the modulus of elasticity at crack tip position.

6. STUDIED CASE

A center cracked plate made of FGM with two different material gradations (along and normal to the crack length) under the effect of step load are considered here. For each gradation, three different lengths are assumed for FGM zone (10% or edge, half and full plate length), hence the following six distinct problems are studied (Fig.2):

- (a) Material gradation along the crack with full gradation (ACFG), half gradation (ACHG) and edge gradation (ACEG).
- (b) Material gradation normal to the crack with full gradation (NCFG), half gradation (NCHG) and edge gradation (NCEG).

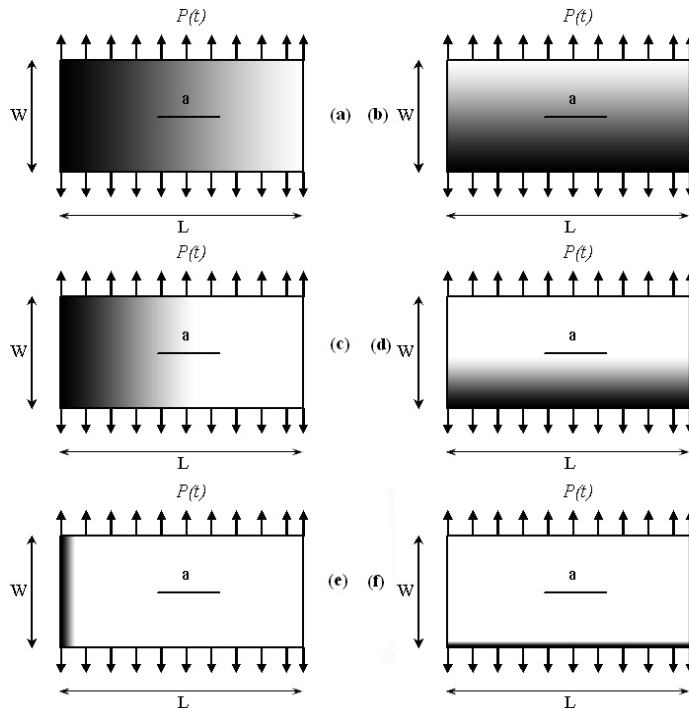


Fig. 2. A center cracked plate, in which material is (a)along the crack with full gradation (ACFG) (b)normal to the crack with full gradation (NCFG) (c)along the crack with half gradation (ACHG) (d)normal to the crack with half gradation (NCHG) (e)along the crack with edge gradation (ACEG) (f)normal to the crack with edge gradation (NCEG)

All problems are solved for period up to $20(\mu s)$ and the time history of the NDSIF of mode-I ($K_I / P\sqrt{a\pi}$) and mode -II ($K_{II} / P\sqrt{a\pi}$) is calculated for the different values of E_2 / E_1 .

The following are the plate specifications which are used in the analyses:

$L=104\text{mm}$, $W=40\text{mm}$, $a=24\text{mm}$, $E_1=76\text{GPa}$, $\nu=0.286$, $\rho_1=2450\text{Kg}/\text{m}^3$

$$P(t) = 0.4H(t) = \begin{cases} 0.4 & t > 0 \\ 0 & t \leq 0 \end{cases} (\text{GPa})$$

and all initial values at $t=0(\text{s})$ are zero.

To validate the method, the homogenous center cracked plate problem ($E_2/E_1=1$) is analyzed first. In Fig. 3 the MLPG results with different nodes are compared with the analytical solution for an infinite plate [34]. The figure shows good agreement between the MLPG results and the analytical solution in the studied homogenous center cracked plate. As the graph demonstrates, the value of NDSIF remains zero up to approximately $t=2.5(\mu\text{s})$, when the dilatational wave reaches the crack. The value of NDSIF then fluctuates and finally converges to a specific value which is approximately equal to static stress intensity factor. Comparison between the converged value and the analytical static solution [35] shows good agreement, too.

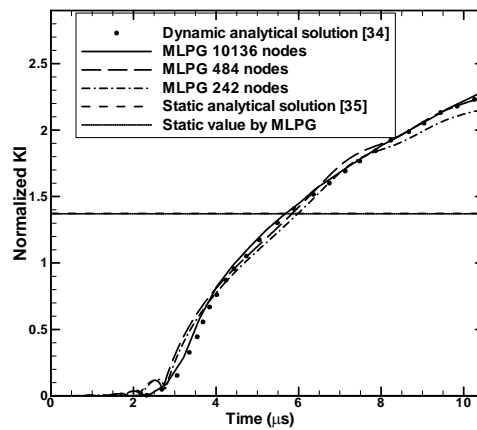


Fig. 3. The time history of the normalized stress intensity factor $K_I / P\sqrt{a\pi}$ for homogenous center cracked plate by MLPG and analytical methods up to time 11 (μs)

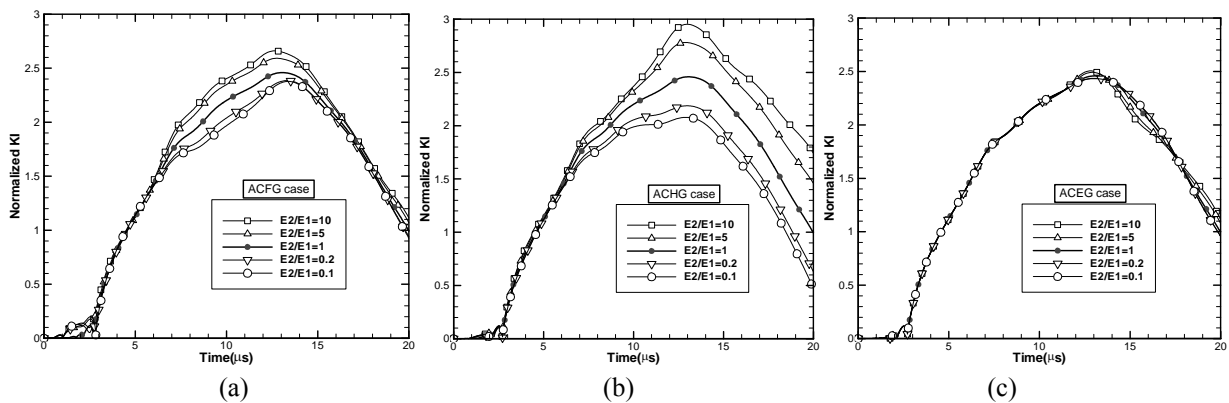


Fig. 4. The time history of the normalized stress intensity factor $K_I / P\sqrt{a\pi}$ for different values of E_2/E_1 (a) ACFG case (b) ACHG case (c) ACEG case

In Fig. 4, the time history of the $K_I / P\sqrt{a\pi}$ for various amount of E_2/E_1 is plotted for ACFG, ACEG and ACEG cases. The graphs show that the increase in E_2/E_1 ratio will cause the value of NDSIF to increase, but for the ACEG case the variation of NDSIF is small. From Fig. 4 it can be observed that the change in gradation direction normal to the crack has no effect on KI and KII distribution which would be expected physically, as the crack is located in the middle of the plate. In Figs 5 & 6, for different values of E_2/E_1 , NCFG, NCHG and NCEG cases the time history of the NDSIF of mode -I and mode -II is plotted, respectively. The converged (normalized static stress intensity factor) and peak (time is about 12 μs)

values of $K_I / P\sqrt{a\pi}$ and $K_{II} / P\sqrt{a\pi}$ in terms of different E_2 / E_1 for ACFG, ACHG, ACEG, NCFG, NCHG and NCEG cases are listed in Table 1. From Figs 4 & 5 and Table 1 it can be observed that in half of the cases, NDSIF is the maximum value for $E_2 / E_1 > 1$ and the minimum value for $E_2 / E_1 < 1$.

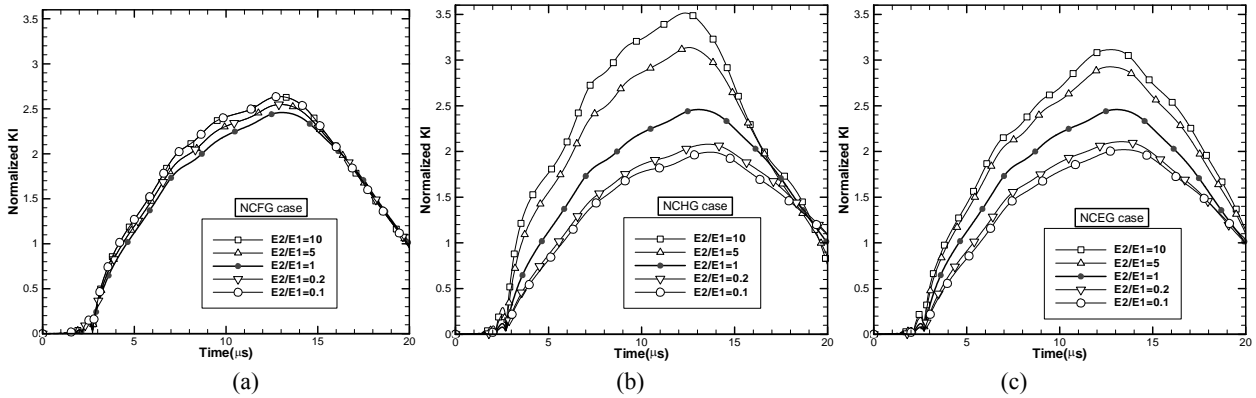


Fig. 5. The time history of the normalized stress intensity factor $K_I / P\sqrt{a\pi}$ for different values of E_2 / E_1 (a) NCFG case (b) NCHG case (c) NCEG case

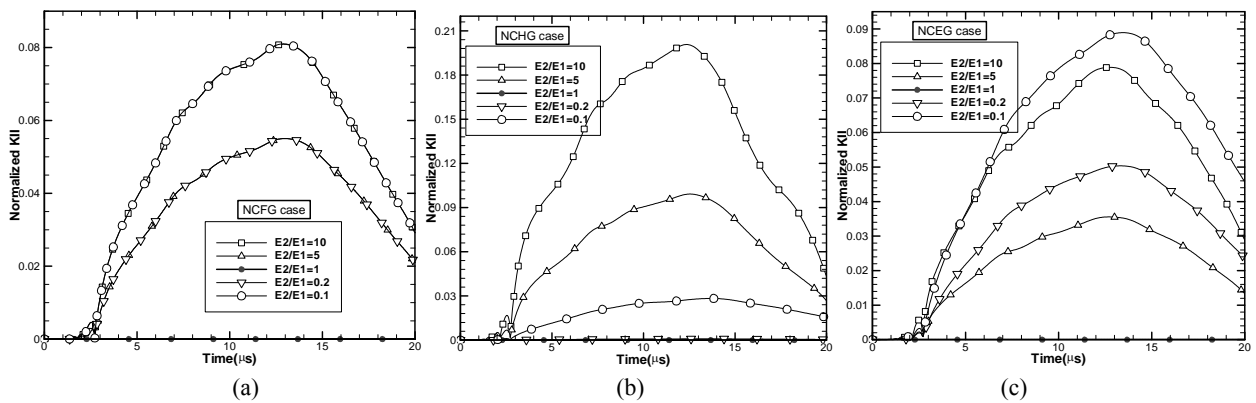


Fig. 6. The time history of the normalized stress intensity factor $K_{II} / P\sqrt{a\pi}$ for different values of E_2 / E_1 (a) NCFG case (b) NCHG case (c) NCEG case

Table 1. The converged and peak (about 12 microseconds) values of dynamic NSIF Mode I and II in terms of different E_2 / E_1 for ACFG, ACHG, ACEG, NCFG, NCHG and NCEG, cases

E2/E1	0.1		0.2		1		5		10	
	Converged value	Peak value								
ACFG- K_I	1.29	2.232	1.320	2.269	1.397	2.394	1.486	2.550	1.527	2.621
ACHG- K_I	1.229	2.041	1.279	2.143	1.397	2.394	1.527	2.697	1.588	2.832
ACEG- K_I	1.404	2.386	1.403	2.386	1.397	2.394	1.389	2.416	1.385	2.431
NCFG- K_I	1.471	2.573	1.433	2.484	1.397	2.394	1.433	2.484	1.471	2.573
NCHG- K_I	1.099	1.887	1.165	1.991	1.397	2.394	1.754	3.105	1.944	3.496
NCEG- K_I	1.144	1.951	1.198	2.048	1.397	2.394	1.660	2.889	1.764	3.082
NCFG- K_{II}	0.093	0.079	0.060	0.054	0	0	0.060	0.054	0.093	0.079
NCHG- K_{II}	0.017	0.027	0.024	0.001	0	0	0.111	0.098	0.225	0.200
NCFG- K_{II}	0.067	0.086	0.045	0.049	0	0	0.006	0.035	0.008	0.078

7. CONCLUSION

In this paper, the meshless local Petrov-Galerkin method is used to analyze the dynamic fracture of an isotropic FGM plate containing a center crack. The time history of the normalized dynamic stress intensity factor of modes I and II in the center cracked plate with two different material gradations (along and normal to the crack length) and three different lengths of FGM zone (10%, half and full plate length) under the effect of step load are studied.

The obtained results show a good agreement between the analytical solution and the MLPG results for homogenous material. For the three different FGM zones that are studied here, the extreme values of NDSIF occurred in the half-length case; when the hardening ($E_2 / E_1 > 1$) behavior was applied, the maximum value and the minimum value obtained in softening FGMs ($E_2 / E_1 < 1$) are given.

The increase in E_2 / E_1 ratio causes the value of normalized dynamic stress intensity factor (NDSIF) to increase. The results demonstrated that in the NCFG case the use of hardening or softening behavior has no effect on KI and KII distribution. This is because of the location of the studied crack, which is in the middle of the plate, and so this would be a physically expectable result.

For the ACEG case, the material gradation has a negligible effect on NDSIF, however, this effect is significant for the NCEG case.

REFERENCES

1. Schwartz, M. (2002). *Encyclopedia of smart material*. John Wiley & Sons, Inc.
2. Shiota, I. & Miyamoto, Y. (1997). *Functionally graded materials 1996*. ELSEVIER SCIENCE B.V.
3. Shukla, A. (2006). *Dynamic fracture mechanics*. World Scientific Publishing Co.
4. Tohgo, K., Sakaguchi, M. & Ishii, H. (1996). Applicability of fracture mechanics in strength evaluation of functionally graded materials. *JSME International Journal Series A*, Vol. 39, No. 4, pp. 479-488.
5. Eischen, J. W. (1987). Fracture of nonhomogeneous materials. *Int. J. Fract.*, Vol. 34, No.3.
6. Chen, J., Wu, L. & Du, S. (2000). A modified J integral for functionally graded materials. *Mech. Res. Commun.*, Vol. 27, No. 3, pp. 301-306.
7. Javanmard, S.A.S., Daneshmand, F., Moshksar, M. M. & Ebrahimi, R. (2011). Meshless analysis of backward extrusion by natural element method. *Iranian Journal of Science and Technology, Transactions of Mechanical Engineering*, Vol. 35, No. M2, pp. 167-180.
8. Gu, P., Dao, M. & Asaro, R. J. (1999). A simplified method for calculating the crack tip field of functionally graded materials using the domain integral. *Journal of Applied Mechanics*, Vol. 66, pp. 101-108.
9. Marur, P. R. & Tippur, H. V. (2000). Numerical analysis of crack-tip fields in functionally graded materials with a crack normal to the elastic gradient. *International Journal of Solids and Structures*, Vol. 37, pp. 5353-5370.
10. Liu, G. R. (2002). *Mesh free methods moving beyond the finite element method*. CRC Press.
11. Atluri, S. N. & Zhu, T. L. (1998). A new Meshless Local Petrov-Galerkin (MLPG) approach in computational mechanics. *Comp. Mech.*, Vol. 22, pp. 117-127.
12. Ching, H. K. & Batra, R. C. (2001). Determination of crack tip fields in linear elastostatics by the Meshless Local Petrov-Galerkin (MLPG) method. *Computer Modeling in Engineering & Sciences*, Vol. 2, No. 2, pp. 273-289.
13. Abdollahifar, A., Shafiei, A. R., Mohyeddin, A. & Bozorg, M. (2010). Using state-space models for solving elastodynamic problems discretized by the MLPG method. *Engineering Analysis with Boundary Elements*, Vol. 34, No. 8, pp. 721-726.
14. Kaiyuan, L., Shuyao, L. & Guangyao, L. A simple and less-costly meshless local Petrov-Galerkin (MLPG) method for the dynamic fracture problem. *Engineering Analysis with Boundary Elements*, Vol. 30, pp. 72-76.
15. Atluri, S. N. & Shen, S. P. (2002). *The Meshless Local Petrov-Galerkin (MLPG) method*. Tech. Science Press.

16. Abdollahifar, A., Nami, M. R. & Shafiei, A. R. (2012). A new MLPG method for elastostatic problems. *Engineering Analysis with Boundary Elements*, Vol. 36, pp. 451-457.
17. Sladek, J., Sladek, V., Zhang, Ch. & Tan, C.H.L. (2006). Evaluation of fracture parameters for crack problems in FGM by a meshless method. *Theoretical and applied mechanics*, Vol. 44, No. 3, pp. 603-636.
18. Koochkan, H., Baradaran, G. H. & Vaghefi, R. (2010). A completely meshless analysis of cracks in isotropic functionally graded materials. *Journal of Mechanical Engineering Science*, Vol. 224, No. 3, pp. 581-590.
19. Abdollahifar, A. & Nami, M. R. (2013). Investigating the effect of angle between the material gradation direction and crack on mixed-mode stress intensity factor of FGM plates using MLPG method. *Modares Mechanical Engineering*, Vol. 13, No. 1, pp. 138-150.
20. Abdollahifar, A. & Nami, M. R. (2013). FGM gradation direction effects on mixed-mode crack initiation angle by MLPG method. *Mechanics Based Design of Structures and Machines: An International Journal*, In press DOI: 10.1080/15397734.2013.853594.
21. Sladek, J., Sladek, V. & Zhang, Ch. (2008). Evaluation of the stress intensity factors for cracks in continuously nonhomogeneous solids, part I: Interaction integral. *Mechanics of Advanced Materials and Structures*, Vol. 15, pp. 438-443.
22. Sladek, J., Sladek, V. & Zhang, Ch. (2008). Evaluation of the stress intensity factors for cracks in continuously nonhomogeneous solids, part II: Meshless method. *Mechanics of Advanced Materials and Structures*, Vol. 15, pp. 444-452.
23. Sladek, J., Sladek, V. & Zhang, C. (2005). The MLPG method for crack analysis in anisotropic functionally graded materials. *Structure Integrity Durability*, Vol. 1, No. 2, pp. 131-144
24. Soares, D., Sladek, Jr. V. & Sladek, J. (2012). Modified meshless local Petrov-Galerkin formulations for elastodynamics. *Int. J. Numer. Meth. Eng.*, Vol. 90, No. 12, pp. 1508-1828.
25. Shukla, A., Jain, N. & Chona, R. (2007). A review of dynamic fracture studies in functionally graded materials. *Strain*, Vol. 43, No. 2, pp. 76-95.
26. Atluri, S. N. & Zhu, T. (1998). A new Meshless Local Petrov-Galerkin (MLPG) approach to nonlinear problems in computer modeling and simulation. *Computer Modeling and Simulation in Engineering*, Vol. 3, No. 3, pp. 187-196.
27. Sladek, V., Sladek, J. & Zhang, Ch. (2010). On increasing computational efficiency of local integral equation method combined with meshless implementations CMES: Computer Modeling. *Engineering & Sciences*, Vol. 63, No. 3, pp. 243-264.
28. Sladek, V. & Sladek, J. (2010). Local integral equations implemented by MLS-approximation and analytical integrations. *Engineering Analysis with Boundary Elements*, Vol. 34, pp. 904-913
29. Soares, Jr., Sladek, V. & Sladek, J. (2012). Modified meshless local Petrov-Galerkin formulations for elastodynamics. *Int. J. Numer. Meth. Engng*, Vol. 90, No. 12, pp. 1508-1828.
30. Fleming, M., Chu, Y., Moran, B. & Belytschko, T. (1997). Enriched element-free Galerkin methods for crack tip fields. *International Journal for Numerical Methods in Engineering*, Vol. 40, pp. 1483-1504.
31. Belytschko, T., Lu, Y. Y. & Gu, L. (1994). *Element-free Galerkin methods*. *International Journal for Numerical Methods in Engineering*, Vol. 37, pp. 229-256.
32. Organ, D.J., Fleming, M. & Belytschko, T. (1996). Continuous meshless approximations for nonconvex bodies by diffraction and transparency. *Comput. Mech.*, Vol. 18, pp. 225-235.
33. Dufloot, M. & Nguyen-Dang, H. (2004). A meshless method with enriched weight functions for fatigue crack growth. *International Journal for Numerical Methods in Engineering*, Vol. 59, pp. 1945-1961.
34. Baker, B. R. (1962). Dynamic stresses created by a moving crack. *Journal of Applied Mechanics*, Vol. 29 pp. 449-455.
35. Fett, T. (2008). *Stress intensity factors – t-stresses – weight functions*. Institute of Ceramics in Mechanical Engineering (IKM), University of Karlsruhe (TH).